Photometric Properties of Jupiter Trojans Detected by the Dark Energy Survey

Jiaming Pan (潘嘉明)[1,2], Hsing Wen Lin (林省文)[2], David W. Gerdes[1,2], Kevin J. Napier[2], Jichi Wang (王骥驰)[2],
T. M. C. Abbott[3], M. Aguena[4], S. Allam[5,43], O. Alves[2,4], D. Bacon[6], P. H. Bernardinelli[7], G. M. Bernstein[8],
E. Bertin[9,10], D. Brooks[11], D. L. Burke[12,13], A. Carnero Rosell[4,14,15], M. Carrasco Kind[16,17], J. Carretero[18],
M. Costanzi[19,20,21], L. N. da Costa[4], M. E. S. Pereira[22], J. De Vicente[23], S. Desai[24], P. Doel[11], I. Ferrero[25], D. Friedel[16],
J. Frieman[5,26], J. García-Bellido[27], M. Gatti[8], R. A. Gruendl[16,17], J. Gschwend[4,28], K. Herner[5], S. R. Hinton[29],
D. L. Hollowood[30], K. Honscheid[31,32], D. J. James[33], K. Kuehn[34,35], N. Kuropatkin[5], M. March[8], F. Menanteau[16,17],
R. Miquel[18,36], F. Paz-Chinchón[16,37], A. Pieres[4,28], A. A. Plazas Malagón[38], M. Raveri[8], M. Rodriguez-Monroy[23],
A. K. Romer[39], E. Sanchez[23], M. Schubnell[2], I. Sevilla-Noarbe[23], M. Smith[40], E. Suchyta[41], G. Tarle[2],
D. Tucker[5], A. R. Walker[3], and N. Weaverdyck[2,42]

[1] Department of Astronomy, University of Michigan, Ann Arbor, MI 48109, USA
[2] Department of Physics, University of Michigan, Ann Arbor, MI 48109, USA
[3] Cerro Tololo Inter-American Observatory, NSF's National Optical-Infrared Astronomy Research Laboratory, Casilla 603, La Serena, Chile
[4] Laboratório Interinstitucional de e-Astronomia—LIneA, Rua Gal. José Cristino 77, Rio de Janeiro, RJ—20921-400, Brazil
[5] Fermi National Accelerator Laboratory, P.O. Box 500, Batavia, IL 60510, USA
[6] Institute of Cosmology and Gravitation, University of Portsmouth, Portsmouth, PO1 3FX, UK
[7] Astronomy Department, University of Washington, Box 351580, Seattle, WA 98195, USA
[8] Department of Physics and Astronomy, University of Pennsylvania, Philadelphia, PA 19104, USA
[9] CNRS, UMR 7095, Institut d'Astrophysique de Paris, F-75014, Paris, France
[10] Sorbonne Universités, UPMC Univ Paris 06, UMR 7095, Institut d'Astrophysique de Paris, F-75014, Paris, France
[11] Department of Physics & Astronomy, University College London, Gower Street, London, WC1E 6BT, UK
[12] Kavli Institute for Particle Astrophysics & Cosmology, P.O. Box 2450, Stanford University, Stanford, CA 94305, USA
[13] SLAC National Accelerator Laboratory, Menlo Park, CA 94025, USA
[14] Instituto de Astrofisica de Canarias, E-38205 La Laguna, Tenerife, Spain
[15] Universidad de La Laguna, Dpto. Astrofísica, E-38206 La Laguna, Tenerife, Spain
[16] Center for Astrophysical Surveys, National Center for Supercomputing Applications, 1205 West Clark Street, Urbana, IL 61801, USA
[17] Department of Astronomy, University of Illinois at Urbana-Champaign, 1002 W. Green Street, Urbana, IL 61801, USA
[18] Institut de Física d'Altes Energies (IFAE), The Barcelona Institute of Science and Technology, Campus UAB, E-08193 Bellaterra (Barcelona), Spain
[19] Astronomy Unit, Department of Physics, University of Trieste, via Tiepolo 11, I-34131 Trieste, Italy
[20] INAF-Osservatorio Astronomico di Trieste, via G.B. Tiepolo 11, I-34143 Trieste, Italy
[21] Institute for Fundamental Physics of the Universe, Via Beirut 2, I-34014 Trieste, Italy
[22] Hamburger Sternwarte, Universität Hamburg, Gojenbergsweg 112, D-21029 Hamburg, Germany
[23] Centro de Investigaciones Energéticas, Medioambientales y Tecnológicas (CIEMAT), Madrid, Spain
[24] Department of Physics, IIT Hyderabad, Kandi, Telangana 502285, India
[25] Institute of Theoretical Astrophysics, University of Oslo. P.O. Box 1029 Blindern, NO-0315 Oslo, Norway
[26] Kavli Institute for Cosmological Physics, University of Chicago, Chicago, IL 60637, USA
[27] Instituto de Fisica Teorica UAM/CSIC, Universidad Autonoma de Madrid, E-28049 Madrid, Spain
[28] Observatório Nacional, Rua Gal. José Cristino 77, Rio de Janeiro, RJ—20921-400, Brazil
[29] School of Mathematics and Physics, University of Queensland, Brisbane, QLD 4072, Australia
[30] Santa Cruz Institute for Particle Physics, Santa Cruz, CA 95064, USA
[31] Center for Cosmology and Astro-Particle Physics, The Ohio State University, Columbus, OH 43210, USA
[32] Department of Physics, The Ohio State University, Columbus, OH 43210, USA
[33] Center for Astrophysics, Harvard & Smithsonian, 60 Garden Street, Cambridge, MA 02138, USA
[34] Australian Astronomical Optics, Macquarie University, North Ryde, NSW 2113, Australia
[35] Lowell Observatory, 1400 Mars Hill Road, Flagstaff, AZ 86001, USA
[36] Institució Catalana de Recerca i Estudis Avançats, E-08010 Barcelona, Spain
[37] Institute of Astronomy, University of Cambridge, Madingley Road, Cambridge CB3 0HA, UK
[38] Department of Astrophysical Sciences, Princeton University, Peyton Hall, Princeton, NJ 08544, USA
[39] Department of Physics and Astronomy, Pevensey Building, University of Sussex, Brighton, BN1 9QH, UK
[40] School of Physics and Astronomy, University of Southampton, Southampton, SO17 1BJ, UK
[41] Computer Science and Mathematics Division, Oak Ridge National Laboratory, Oak Ridge, TN 37831, USA
[42] Lawrence Berkeley National Laboratory, 1 Cyclotron Road, Berkeley, CA 94720, USA

Abstract

The Jupiter Trojans are a large group of asteroids that are coorbiting with Jupiter near its L4 and L5 Lagrange points. The study of Jupiter Trojans is crucial for testing different models of planet formation that are directly related to our understanding of solar system evolution. In this work, we select known Jupiter Trojans listed by the Minor Planet Center from the full six years data set (Y6) of the Dark Energy Survey (DES) to analyze their

---

[43] Deceased.

photometric properties. The DES data allow us to study Jupiter Trojans with a fainter magnitude limit than previous studies in a homogeneous survey with *griz* band measurements. We extract a final catalog of 573 unique Jupiter Trojans. Our sample include 547 asteroids belonging to L5. This is one of the largest analyzed samples for this group. By comparing with the data reported by other surveys we found that the color distribution of L5 Trojans is similar to that of L4 Trojans. We find that L5 Trojans' $g - i$ and $g - r$ colors become less red with fainter absolute magnitudes, a trend also seen in L4 Trojans. Both the L4 and L5 clouds consistently show such a color–size correlation over an absolute magnitude range $11 < H < 18$. We also use DES colors to perform taxonomic classifications. C- and P-type asteroids outnumber D-type asteroids in the L5 Trojans DES sample, which have diameters in the 5–20 km range. This is consistent with the color–size correlation.

Unified Astronomy Thesaurus concepts: Asteroids (72); Jupiter trojans (874); Trojan asteroids (1715)

Supporting material: machine-readable table

1. Introduction

The properties of Jupiter Trojans, small bodies that populate the 1:1 mean motion resonance near Jupiter's L4 and L5 Lagrange points, encode important clues about the processes that shaped our solar system and its origins. Recent theories, e.g., the Nice Model (Morbidelli et al. 2005), Grand Tack (Walsh et al. 2011), and Jumping Jupiter (Nesvorny et al. 2013; Roig & Nesvorný 2015) support the idea that radial migrations have happened in the early solar system. Under this hypothesis, Jupiter Trojans reached their current orbits by scattering inward from the primordial planetesimal disk as the giant planets migrated outward. Thus, the Trojans may share the same origin as Kuiper Belt objects in this scenario.

The alternative hypothesis suggests that it is also possible for Jupiter Trojans to form in their current locations by capturing planetesimals during the formation of Jupiter (Marzari & Scholl 1998; Fleming & Hamilton 2000). Consequently, their relations with trans-Neptunian objects (TNOs) and other small-body populations, e.g., Hildas and main-belt asteroids (MBAs), contain crucial implications for the solar systems formation hypothesis (TNO: Morbidelli et al. 2009; Fraser et al. 2014, Hildas: Wong et al. 2017, MBAs: Yoshida et al. 2019).

Over the last few decades, numerous observations, experiments, and analyses related to Jupiter Trojans have considerably deepened our understanding of their physical properties, including sizes, colors, and taxonomic types. However, our knowledge of the underlying mechanics and compositions responsible for those properties remains poorly constrained (Wong et al. 2019). With the upcoming exploration of Lucy spacecraft (Levison et al. 2021), further analysis of the Jupiter Trojans is an even more compelling task.

Jupiter Trojans have several important features. The color bimodality of Trojans has been claimed in many previous studies in both spectroscopic and photometric surveys (Szabó et al. 2007; Roig et al. 2008; Wong et al. 2014; Wong & Brown 2015). Szabó et al. (2007) analyzed 869 unique Jovian Trojans in the Sloan Digital Sky Survey Moving Object Catalogue third release. They found that the colors of Trojans have small scatters and are correlated with orbital inclination. Emery et al. (2011) identified two compositional groups in the Jovian Trojan population using near-infrared spectra, which shows two distinct "red" and "less-red" groups. Wong et al. (2014) found that the "red" and "less-red" groups show different magnitude distributions. Wong & Brown (2015) showed that there are more "less-red" Trojans in $g - i$ colors with decreasing sizes in the L4 clouds. Furthermore, Wong et al. (2019) reported distinct UV spectral shapes between the "red" and "less-red" Trojans.

Large-scale photometric surveys can statistically study the color and taxonomic type of Trojans, and these properties are indicators of the surface composition of Jupiter Trojans, or even more, can be used as the parameters to identify possible collisional families (Holt et al. 2021). Previously, the Sloan Digital Sky Survey (SDSS; Ivezić et al. 2001, 2002), WISE (Mainzer et al. 2011), SkyMapper (Sergeyev et al. 2022), and VISTA (Popescu et al. 2016, in near-infrared) have studied surface properties for a large number of Jupiter Trojans. However, these surveys are generally biased toward Trojans with large sizes (usually bigger than diameters of 20 km). Suprime-Cam (SC) and Hyper Suprime-Cam (HSC), which are mounted on the 8 m class Subaru telescope, have reached deeper magnitudes and have given insights into the magnitude distributions (Yoshida & Nakamura 2005, 2008; Yoshida & Terai 2017; Uehata et al. 2022) and color–magnitude relation of small Trojans (Wong & Brown 2015). However, those surveys generally lack the multiple band measurements that enable the measurement of taxonomic types.

This study, carried out with data from the Dark Energy Survey (DES; DES Collaboration 2005) reaches a deeper magnitude limit, ∼15 in absolute magnitude H_V and correspondingly to $m_V \sim 22$, than the 4th release of Sloan Digital Sky Survey Moving Object Catalogue (SDSS MOC-4; Ivezić et al. 2001, 2002). Also, DES photometry in the g, r, i, and z bands allows the classification of Trojans into different taxonomic types (e.g., Carvano et al. 2010; DeMeo & Carry 2013). The goal of this work is to extend our understanding of the Jupiter Trojans' physical properties at the diameters of 5–20 km (assuming a constant geometric albedo of 0.07 Grav et al. 2011) and use them to shed light on the formation and evolution of Trojans.

This paper presents the photometry of Jupiter Trojan asteroids observed/imaged in the full six year data set from DES. The number of identified L5 Jupiter Trojans is substantially higher than L4 Jupiter Trojans. We present the color distributions of Jupiter Trojans for L5 Trojans. We demonstrate the trend of L5 Trojans' absolute magnitudes with colors, and compared the color–size correlation in different surveys. Finally, we classify these Trojans into different taxonomic classes and further discuss the results' implications.

2. DES Data Set

The DES (DES Collaboration 2005) was an optical survey carried out between 2013 and 2019 using the Dark Energy Camera (DECam; Flaugher et al. 2015) on the 4 m Blanco telescope at Cerro Tololo Inter-American Observatory in Chile. The DES consisted of two interleaved surveys: the wide
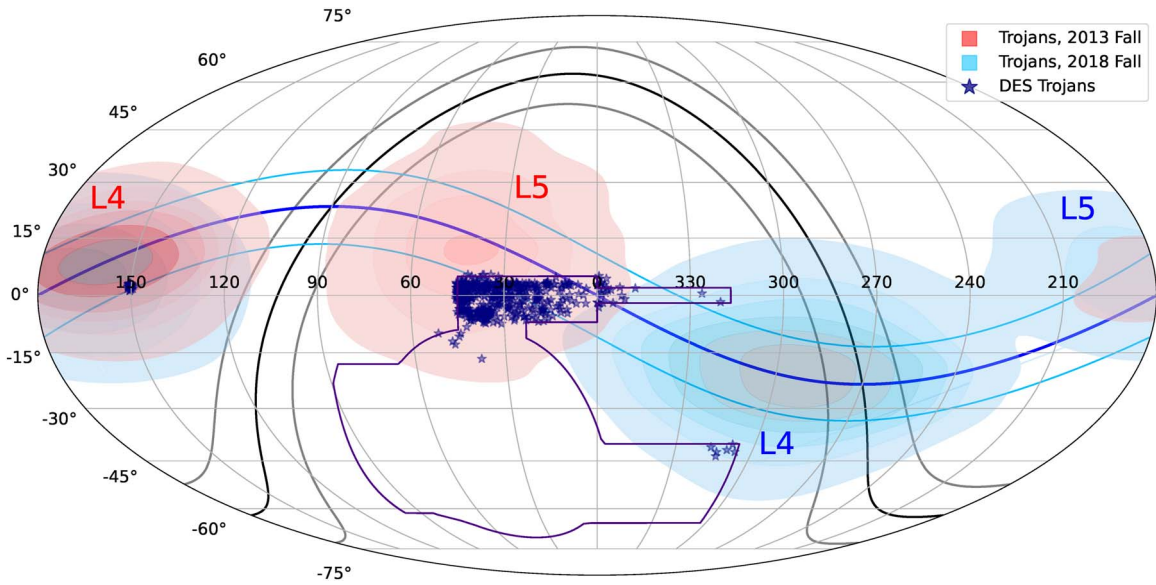
Figure 1. Sky positions of DES observed Jovian Trojans and the DES survey footprint, as well as the ecliptic (blue) and galactic (black) plane. Most of the Trojans belong to L5 camp and were observed during 2013 to 2014. Some L4 Trojans have been picked up in COSMOS field (R.A. ~ 150°) in 2013 or by the main survey in 2018.

survey, which imaged a 5000 sq. deg. area centered upon the north galactic cap in the *grizY* bands to a single-exposure depth of $r \sim 23.8$, and the supernova survey (Bernstein et al. 2012), which imaged ten 3 sq. deg. DECam fields at approximately weekly intervals in the *griz* bands. The photometry system is similar but not identical to the SDSS system,[44] therefore we refer the detail of the photometry data set of DES to Drlica-Wagner et al. (2018). Though intended primarily as a cosmological survey, the DES's combination of a large survey area, multiyear time baseline, and single-exposure depth make it an outstanding tool for studying our solar system. DES has yielded discoveries of hundreds of new Kuiper Belt Objects (Bernardinelli et al. 2020, 2022; Khain et al. 2020), a dwarf planet candidate at 92 au (Gerdes et al. 2017), several Neptune Trojans including the first ultrared member of this population (Gerdes et al. 2016; Lin et al. 2019), and a giant Oort cloud comet (Bernardinelli et al. 2021). Despite the survey's success in discovering new outer solar system objects, a search for new Jupiter Trojans is prohibitively expensive due to its computational complexity (Bernardinelli et al. 2022). Still, we were able to identify individual detections of known Trojans in the DES data (most Trojans have multiple individual detections).

The present work makes use of the 107,631 calibrated single-exposure images and catalogs that comprise the full DES six year (Y6) data set. These images underlie the coadd images and catalogs that were publicly released in 2021 January as DES DR2 (Abbott et al. 2021). All *griz* exposures are 90 s in duration. The ten supernova fields are distributed within the footprint of DES and have longer exposures.

3. Trojans in the DES Data

This section describes how we extract known Jupiter Trojans listed in the Minor Planet Center (MPC) from the DES Y6 data and further clean the data to get a sample of Trojans with reliable photometry. As of 2021 September, the MPC lists 10,437

objects classified as Jupiter Trojans. First, we identify the exposure/CCD combinations in the DES Y6 data that contain known Trojans. Positional uncertainties of identified objects were estimated and required to be smaller than 2″ in R.A. and decl. to ensure accurate matching in our images. Then, we obtain photometry of these identified objects from a catalog of sources detected in individual exposures in the DES Y6 data, excluding objects with nearby stationary objects. We derive absolute magnitudes H of these Trojans. Finally, we further constrain these objects in the number of single exposure and magnitude uncertainties to get a more reliable catalog of Trojans and photometry. Also, some objects listed as known Trojans are not long-term stable, and they are removed as described in Section 3.3 below.

3.1. Identifying Trojans in Y6 of Data from DES

The Trojans in the MPC are complete to around absolute magnitude H of 14 on 2019 September 29 (Hendler & Malhotra 2020). Only DES Y6 exposures with ecliptic latitude from $-30°$ to $30°$ are searched. We obtain the orbital elements of known Trojans from the MPC and use the SPACEROCKS package (Napier 2020) to propagate each Trojan to the epoch of each DES exposure. The SPACEROCKS ephemerides generally agree with JPL Horizons to better than $0.″2$ for the numbered minor planets.[45] If the ephemeris position falls within the DECam field of view, the object is identified as a potential Trojan in the DES Y6 data. After this search, we obtain 13,732 exposures in DES Y6 data containing 1084 unique Trojans. Their sky positions are shown in Figure 1.

3.2. Photometry of Trojans

We cross-match these 1084 objects to sources detected in single exposures in the DES Y6 data with a separation smaller than 2″. To avoid contamination from stationary sources that happen to coincide with the predicted position of a Trojan, we

---

Table 1
The Final Catalog of Jupiter Trojans in the Six Years Data Set of DES

Column Name	Unit	Description
Name		MPC Designation
H_g	mag	Absolute magnitude in g band
σ_g	mag	Uncertainty in H_g
H_r	mag	Absolute magnitude in r band
σ_r	mag	Uncertainty in H_r
H_i	mag	Absolute magnitude in i band
σ_i	mag	Uncertainty in H_i
H_z	mag	Absolute magnitude in z band
σ_z	mag	Uncertainty in H_z
L_n		Assigned cloud (L4 or L5)

(This table is available in its entirety in machine-readable form.)

Table 2
Number of Detected Jupiter Trojans in Different Bands and Cloud

Filter Bands	L5	L4
g	429	14
r	272	14
i	320	21
z	328	18
g, i	206	8
g, r	206	8
r, i	220	10
i, z	192	10
g, r, i	206	8

use the DES coadd catalog (Abbott et al. 2021) as a veto. This catalog is obtained by coadding single images in each band acquired throughout the duration of the survey; coadded sources are therefore presumed to be stationary. Single-exposure detections that fall within $1''$ of a coadd catalog source are excluded, a cut that reliably retains moving objects uncontaminated by stationary sources (Bernardinelli et al. 2020). We make an exception for cases where the coadded source was detected in exactly one of its constituent images, as this could arise from a sufficiently bright moving object. At this stage, we reach 888 unique Trojans with 12,057 exposures.

Absolute magnitudes (H) of Trojans in each exposure are derived from apparent magnitude using the distances and phase angles at the epoch of exposure. The relation between apparent and absolute magnitude is

$$m = H + 5 \log_{10}\left(\frac{r\Delta}{d_0^2}\right) - 2.5 \log_{10} q(\alpha), \quad (1)$$

where r and Δ are heliocentric and geocentric distance, respectively. The d_0 is 1 au, and $q(\alpha)$ is the phase integral. We chose the standard HG model with $G = 0.15$.

Once we derived the H for each object in each epoch in each band, the weighted means of H in each specific band are taken as the final value for absolute magnitude, which is

$$H = \frac{\sum_{i=1}^{n} \frac{H_i}{\sigma_i^2}}{\sum_{i=1}^{n} \frac{1}{\sigma_i^2}}, \quad (2)$$

where i indicates the individual detection in the specific band for the specific object. We sum over the number of detection of each Trojan in each epoch and each band and the uncertainty is

$$\sigma = \sqrt{\sigma_0^2 + \left(-\frac{2.5}{\ln(10)} \frac{\sigma_{\text{flux}}}{\text{flux}}\right)^2}, \quad (3)$$

where the σ_0 is the value of zero-point magnitude uncertainties and it is usually around 0.002 mag. Through standard error propagation, Equation (3) includes both zero-point magnitude uncertainties and apparent magnitude uncertainties which are estimated using *flux* and *flux* uncertainties (σ_{flux}) from DES Y6 data. The uncertainty for the absolute magnitudes of each

Trojan in each band is

$$\overline{\sigma}^2 = \frac{1}{\sum_{i=1}^{n} \frac{1}{\sigma_i^2}}. \quad (4)$$

Note that we do not include uncertainty from rotational light-curve variability here as we do not have enough data on each Trojan to estimate it. We discuss of the effect of Trojan's rotations further in Section 4.4.

3.3. Further Constraints on the Selected Trojans

We put constraints on the positional uncertainties to ensure that the selected objects are bona fide Trojans. The positional uncertainties are estimated using the JPL Horizons system. Uncertainties for every identified object at the time of its exposure time are estimated. The JPL Horizons system gives 3σ uncertainties around the nominal position in arcseconds. We constrain all Trojans to have positional uncertainties smaller than $2''$ in both R.A. and decl. After this process, we arrive at 9864 individual detections of 775 unique Trojans.

To further improve the quality of our photometry, we require that the number of detections of each Trojan is larger than 1, and the magnitude uncertainty is smaller than 0.1. Moreover, the MPC identifies Trojans automatically using their orbital elements, which is not 100% reliable.[46] We integrate all 584 objects for 10 million years to make sure that they have stable Trojan orbits. We find 11 objects that are not permanently in resonance, indicating a ~2% contamination rate. We remove these 11 objects from the following analysis.

3.4. Final Catalog of Trojans

Finally, we arrive at a final catalog of Jupiter Trojans in the DES Y6 data, which contains 573 unique Trojans. In Table 1, we present this catalog in a machine-readable format. Table 2 shows the number of detected Trojans in different bands and the combination of $\{g, i\}$, $\{g, r\}$, $\{r, i\}$, $\{i, z\}$, and, $\{g, r, i\}$ bands and cloud (L4 and L5). This corresponds to 178 L5 and 8 L4 unique Trojans with measurements in all bands. We present the analysis of this data set in the Section 4.

Some Trojans are not assigned to a cloud by the MPC. We assign these Trojans to L4 (L5) if they lead (trail) Jupiter by more than $20°$ the time of observation.

---

[46] https://www.minorplanetcenter.net/iau/lists/Trojans.html
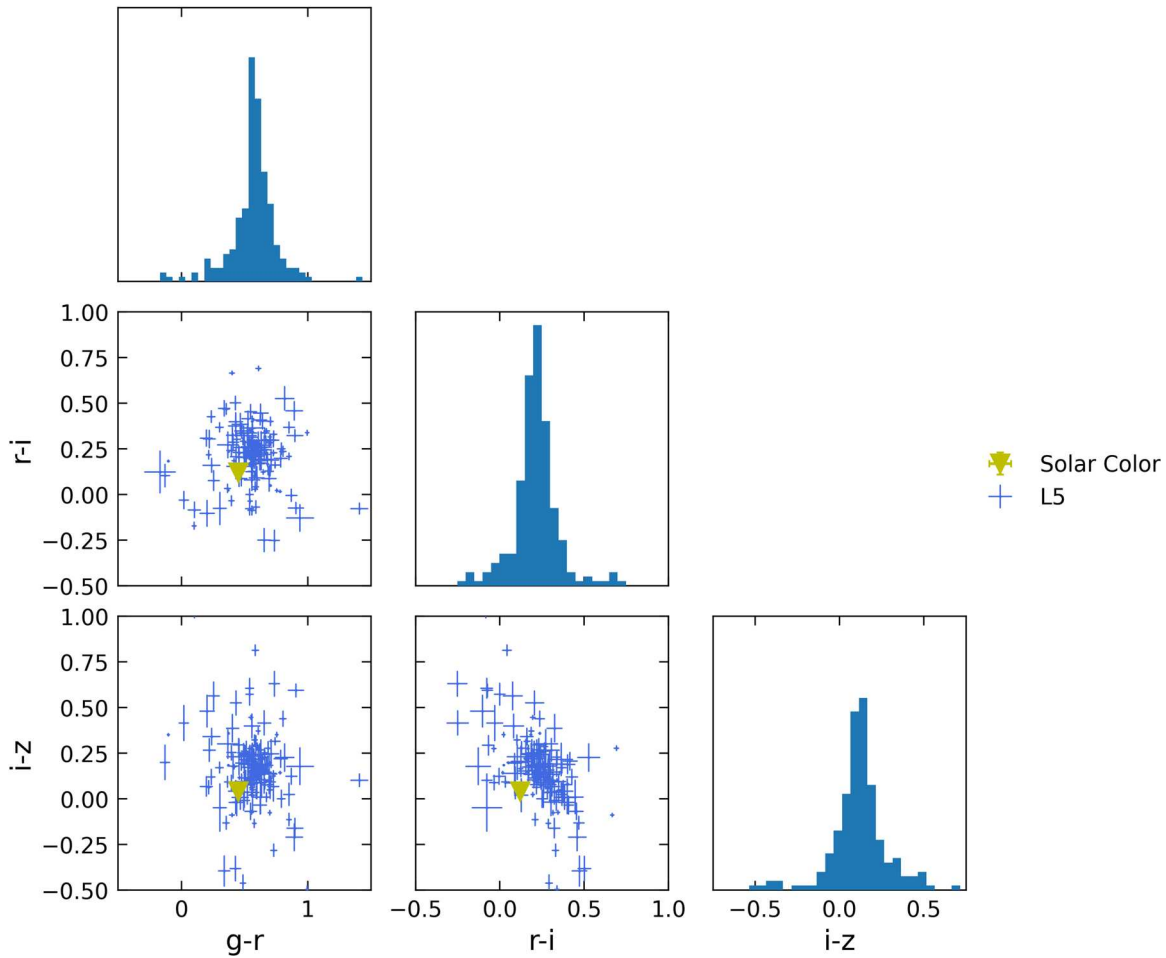
Figure 2. The lower triangle shows Jupiter Trojans' colors for the L5 clouds (blue). The diagonal plots show each color distribution in stacked histograms. The yellow triangle shows the solar color. No bimodality has been found in the colors. L5 Trojans tend to be redder than the solar colors.

4. Results

In this section, we present the results from photometric observations of Trojans in the DES data, including the absolute magnitude distribution, color–color diagram, and correlation between colors and sizes. We further investigate the color–size correlation in a combination of SDSS MOC-4, Subaru, and DES data. To help the comparison among different surveys, the g, r, i, and z-band DES photometric magnitudes were converted to the SDSS photometric scheme using the equations in Appendix A.4 of Drlica-Wagner et al. (2018). Finally, we present the classification of taxonomic types for Trojans.

4.1. Color Distributions of Jupiter Trojans

We show the color distribution of Jupiter Trojans in the diagonal of Figure 2. The colors in $g - r$, $r - i$, and $i - z$ were restricted to between -2 and 2 to eliminate unphysical red or blue colors. The histogram of colors does not show a bimodality even for bright objects, which has been discernible in the SDSS MOC-4 data according to Wong & Brown (2015). We used the unbinned top-hat Kernel Density Estimation method to fit the color distributions and still detect no obvious bimodality. Thus, the lack of bimodality is not an issue with the choice of binning. This could be caused by the smearing of colors due to rotations of Trojans, as was suggested to produce a similar effect in faint L4 Trojans detected by Subaru

survey (Wong & Brown 2015). In particular, the uncertainties introduced by the rotations of Trojans (~ 0.2 mag) is close to the mean color difference between less-red and red groups, where the latter value is 0.13 mag using Trojans in SDSS MOC-4 (Wong & Brown 2015). The standard deviation for $g - r$, $r - i$, and $i - z$ are 0.18, 0.16, and 0.28 respectively for L5 Trojans. Standard deviations of the color distributions are likely to be enlarged by ~ 0.1 mag due to the effects of the rotations of Trojans, which will later be shown in Section 4.4.

Figure 2 lower triangle shows the color–color diagrams of Trojans. The colors are calculated from absolute magnitudes. The color of the Sun is overplotted for comparison (Holmberg et al. 2006). Most L5 Trojans are slightly redder than the Sun in both color–magnitude diagrams. The number of L4 Trojans in our sample is too small, below ten in numbers for each color–color plot, to build a reliable sample. Thus, we do not compare L4 and L5 Trojans in this study. The mean $g - r$, $r - i$, and $i - z$ colors of L5 Trojans are 0.56 ± 0.18, 0.22 ± 0.16, and 0.17 ± 0.28 respectively.

4.2. Sizes and Colors Relation

Here, we use the absolute magnitude to characterize Trojan's size, and study its relation with colors (Figure 3). The mean colors of $g - i$, $g - r$, $i - z$, and $r - i$ are the average of each bin of 1 mag, with uncertainties estimated within the same bin. We estimate the uncertainty in mean color as the standard error
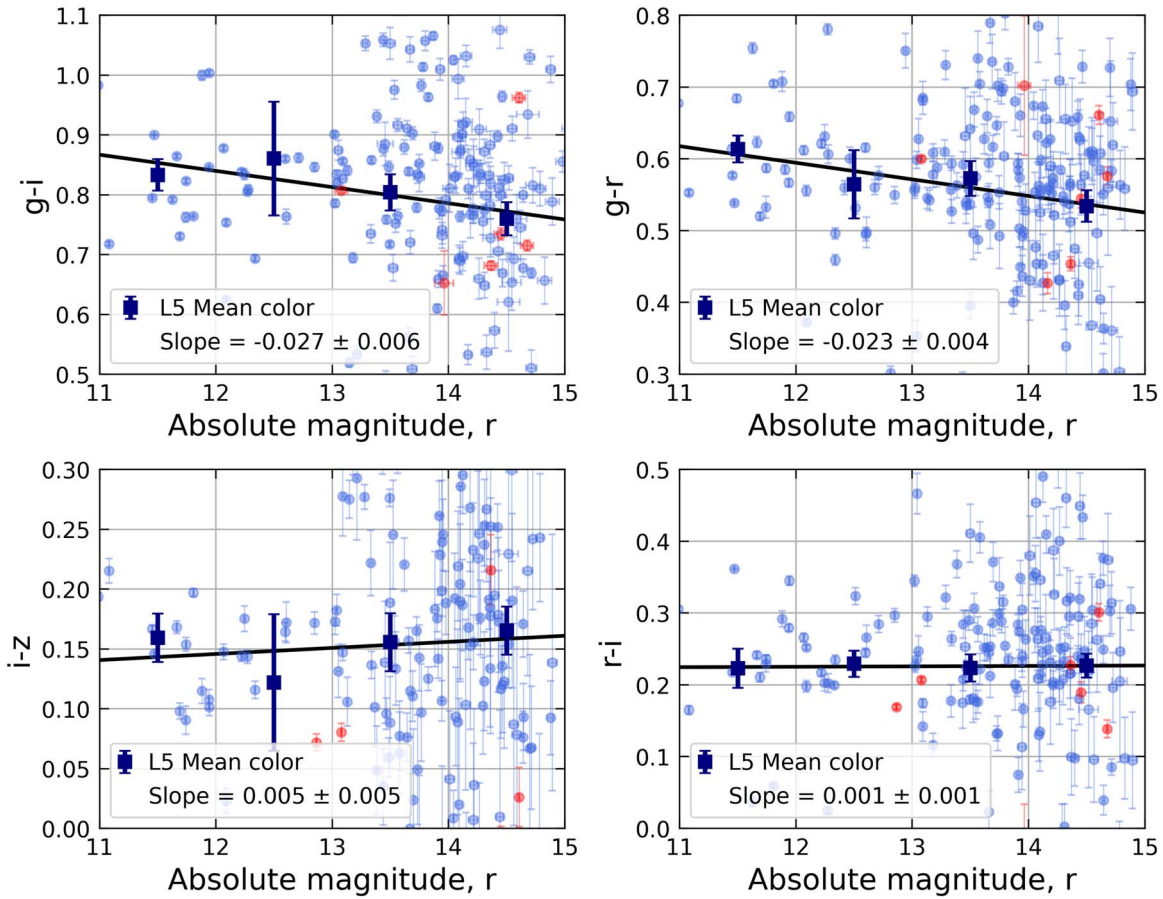
Figure 3. Color–magnitude diagram of Trojans (red and blue dot for L5 and L4 Trojans respectively) and mean $g - i$, $g - r$, $i - z$, and $r - i$ colors of L5 Trojans after changing the size of bin to 1 mag (blue squares). The absolute magnitude is used to estimate the size of Trojans. The mean $g - i$ and $g - r$ colors show a trend of becoming less red with decreasing sizes of L5 Trojans. However, the mean $i - z$ and $r - i$ colors do not show such a trend. The black lines are the best-fitted straight lines, excluding outliers.

in each bin. The absolute magnitude of the r band for the mean colors is restricted to 11–15, beyond which there are only a few data, so we omit them in this case. We also constrain the colors in $g - i$, $g - r$, $r - i$, and $i - z$ to the ranges of $[-0.5, 2]$, $[-0.5, 2]$, $[-0.6, 1]$, and $[-0.5, 0.8]$ respectively to avoid influences from outliers. In a linear fit, there is a clear trend of decreasing mean colors in $g - i$ and $g - r$ of L5 Trojans. The best-fitted lines for the $g - i$ and $g - r$ mean colors have slopes of -0.027 ± 0.006 and -0.023 ± 0.004, respectively. In comparison, the slopes for the $i - z$ and $r - i$ mean colors are 0.005 ± 0.005 and 0.001 ± 0.001 respectively. As a result, the best-fitted lines for $g - i$ and $g - r$ colors are consistent with negative slopes; in contrast, the slopes for $i - z$ and $r - i$ were very close to zero. Such a trend does not disappear if the bin size is changed to 0.5 mag. Also, shifting the center of the bin up by 0.5 mag or to the median of the bin does not significantly change the trend. Furthermore, we used F-test to compare the significance of $y = a + bx$ model and $y = a$ model for the data. F-test suggested that there is a clear linear relationship, i.e., $y = a + bx$ model, for $g - i$ and $g - r$ colors with sizes, but not for $i - z$ and $r - i$ colors. The p-values for $g - i$, $g - r$, $i - z$, and $r - i$ colors with sizes are 0.099, 0.072, 0.398, and 0.884 respectively. This further confirms our findings of the color–size correlation. Here we adopt a p-value to be <0.1 to reject the null hypothesis of no linear relationship. The correlation breaks down when the magnitude is brighter than 10 because only two objects are in that magnitude range. Such correlations

were discovered for the first time in the L5 cloud of Trojans. The $g - i$ colors correlation with sizes agrees with the finding in Wong & Brown (2015), which used only L4 Trojans for their analysis.

However, the DES Trojans were observed at different epochs; the effect of the rotations, which have a typical amplitude of 0.2 mag, may contribute to such a pattern. In Section 4.4 we use simple simulations to show that the negative slopes are still present even when uncertainties from rotations are included. Also, selection effects may create spurious slopes in $g - i$ and $g - r$ colors with sizes. In particular, a different signal-to-noise ratio (S/N) level in one of two filters could mimic a similar relationship in sizes and colors. For example, if g band has a worse S/N than r or i bands, then redder objects become too faint to be detected in the g band at the faint end of magnitudes. In this scenario, the absence of redder objects at the faint ends of the sample would lead to an artificial trend in $g - i$ and $g - r$ colors and sizes. To address this concern, we examine the S/N of Trojans at all filter bands around the magnitude limits. We found that at around S/N of 10 ($0.08 < \sigma_m < 0.14$, where σ_m is magnitude uncertainty) the magnitude median values are $g = 15.2$, $r = 14.5$, $i = 14.4$, and $z = 14.3$. This means that Trojans would have been more reliably detected in the g band than r or i bands, contrary to the potential problematic scenario. Therefore, the color–size correlations are unlikely to be caused by selection effects.
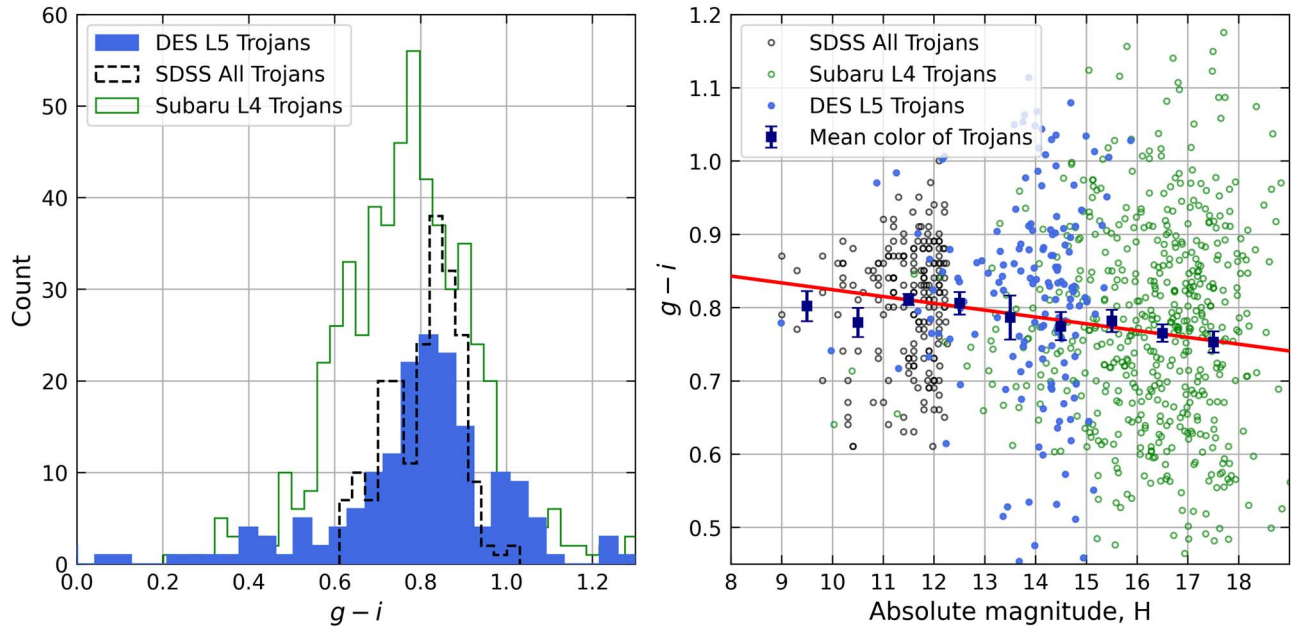
Figure 4. The left panel shows $g - i$ color distributions of Trojans in SDSS MOC-4 catalog, Subaru data, and known Trojans in DES data. DES g and i magnitudes were converted to SDSS magnitudes. The right panel shows the same data in a color absolute magnitude diagram, where the mean of $g - i$ colors in a bin size of 1 mag is overplotted. The fit of mean $g - i$ colors does not include bright Trojans ($H > 11$). The mean $g - i$ colors show a trend of getting less red with fainter magnitudes in DES and Subaru data.

4.3. Comparison with Trojans in Other Surveys

We compared JTs in this study with Trojans in the SDSS MOC-4 and Wong & Brown (2015) (Figure 4). We extracted known Trojans in the SDSS MOC-4 catalog. They lie in the regions with distances from 5.04 to 5.4 au (DeMeo & Carry 2013) and have $e < 0.3$. The absolute magnitude was constrained to be brighter than 12.3, at which the SDSS MOC-4 catalog is almost complete. SDSS MOC-4 contains more Trojans than DES data due to the larger coverage area. Wong & Brown (2015) (hereafter Subaru data) used the Suprime-Cam instrument for the measurement of Trojan colors. The $g - i$ colors in their sample were already calibrated to the SDSS photometric system. We further checked whether the conversion between SDSS and Suprime-Cam magnitudes depends on color, and found that the color terms are almost negligible (see Appendix). Thus, we take $g - i$ colors from Wong & Brown (2015) as SDSS $g - i$ colors. At the absolute magnitude interval from 11 to 13, where SDSS and DES data overlap, the mean $g - i$ color difference between SDSS and DES data is around 0.009 ± 0.04 mag. At absolute magnitude intervals from 13 to 15, the mean $g - i$ color between DES and Subaru data differs by around 0.03 ± 0.06 mag. The offsets between three different data sets are small compared with the dispersion of the data. However, there could still be contributions from some un-calibrated systematic effects other than color terms between the three photometric systems. Therefore, we conservatively shift the offsets, so that the overlapping absolute magnitude intervals of these three samples have the same mean $g - i$ colors. The following analyses would not be driven by the differences among the three photometric systems.

The left panel of Figure 4 shows the histograms of L5 Trojans in the DES data, all the Trojans in the SDSS MOC-4 catalog, and L4 Trojans from Subaru data. The mean colors among the three data sets are very close, with a difference smaller than 0.1 mag. The small peak of DES L5 Trojans at

$g - i$ around 1 mag is likely an artifact caused by the uncertainties in magnitudes, and it disappears at some other choices of binning. We also note that the DES Trojans colors have a larger scatter than SDSS and Subaru Trojans. We maintain that this is an effect caused by the rotations of Trojans, and it will be discussed in Section 4.4. Also, KS tests show that $g - i$ distributions in all three data are not compatible with each other.

Figure 4 right panel shows the mean $g - i$ colors as a function of absolute magnitudes in the V band. The DES reaches a depth in between SDSS and Subaru. We found that the mean $g - i$ colors have a decreasing trend for SDSS, DES, and Subaru data. Mean $g - i$ colors and their uncertainties with a bin size of 1 mag are overplotted. The uncertainty in mean color is estimated in the same way as that of the previous section. Bright Trojans in the SDSS data seem to deviate from this trend ($H > 11$), as they tend to be bluer than the expected correlation. The agreement of these bright Trojans with the trend is sensitive to variations in bin sizes. It is likely that the strong color–size correlation breaks for these bright objects, consistent with finding in Szabó et al. (2007). Further studies are needed to understand why the correlation breaks for these very big Trojans. Note that in the collisional interpretation, the large objects will not follow such a color–size correlation, as they are expected to not form fragments. Further discussion will be in Section 5. The trend of objects at fainter magnitudes still shows a clear decreasing trend at different bin sizes. Regardless of the break at brighter magnitudes, the faint end of SDSS Trojans ($H > 11$) is still consistent with the expected color–size correlation. Also, the mean of the Trojan colors in the SDSS data is redder than both DES and Subaru data, with the mean colors in the Subaru data being the less red. This is also consistent with the correlation. Additionally, we considered SDSS MOC-4 L4 and L5 clouds separately. No significantly different conclusions have been found.

A fitted line for the mean $g - i$ colors, shown as the red line in the right panel of Figure 4, has a slope of -0.009 ± 0.001. Bright Trojans with $H > 11$ are not included in the fit. This slope is around three times smaller than the slope in the $g - i$ color in the DES data (-0.027 ± 0.006). Moreover, we performed a linear fit for L4 Trojans in the Subaru data only with absolute magnitude from 12 to 18 and $g - i$ color from 0.4 to 1.2 to exclude Trojans with color biases and large uncertainties (Wong & Brown 2015). Subaru L4 Trojans have a slope of -0.010 ± 0.001. Similar to the joint data, the slope of Trojans in Subaru data is smaller than that of DES Trojans by around a factor of 3. Nevertheless, a negative slope is still statistically important in the Subaru data within the error bar. Also, both slopes in the red line of Figure 4 right panel and Subaru data are within three sigma away from the DES derived slope. Here we only consider uncertainties in the colors. Thus, we found a similar relation between colors and sizes in DES and Subaru data. The strong correlation persists from faint Trojans (diameters $\lesssim 4$ km or $H \gtrsim 18$) until bright Trojans (diameters $\gtrsim 30$ km or $H \lesssim 11$). Even though we used L4 and L5 Trojans data, which have several differences in physical properties, the color–size correlation is present in both clouds with different magnitude ranges.

4.4. Effects of Asteroid Rotations

As the DES color measurements of the Trojans were not simultaneous, the rotation of the objects needs to be taken into account. The DES measured colors can be described as the following equation:

$$C_{\text{obs}} = C_{\text{true}} + \text{rot} = \bar{C} + \sigma + \text{rot}. \qquad (5)$$

Here, C_{obs} is the color we measured, C_{true} is the true color of the object, $\bar{C}$ is the mean color of the sample, σ is the intrinsic color dispersion from the sample mean of the object, and rot is the rotational effect term, which is the deviation induced by the object rotation. The mean colors we calculated in Sections 4.1 and 4.3 are

$$\langle C_{\text{obs}} \rangle = \frac{1}{n} \sum_{i=1}^{n} (\bar{C} + \sigma_i + \text{rot}_i) = \bar{C} + \langle \sigma \rangle + \langle \text{rot} \rangle. \qquad (6)$$

Here, n is the total number of the sample. By definition, the average of intrinsic color dispersion term $\langle \sigma \rangle$ is zero. If the average of the rotational effect term $\langle \text{rot} \rangle$ is also zero, we have $\langle C_{\text{obs}} \rangle = \bar{C}$.

It is not possible to distinguish the σ and rot from the DES color measurements. Therefore, to test this assumption, we conservatively treated all of the deviations as intrinsic color dispersion and add the additional rotational term to each Trojan. Trojans at the sizes of DES generally have a light-curve amplitude of 0.2 mag (Chang et al. 2021). We assumed that the light curves of Trojans follow a sinusoidal curve with amplitudes randomly drawn from a Gaussian distribution at a mean of 0.2 and a standard deviation of 0.1. We randomly sampled a phase of light curve from 0 to 2π for each observation and add this additional rotation term into the photometric measurements. Applying this step to all the objects, we obtained a new color distribution and a new mean color. After repeating the above steps 100,000 times, we found that the new mean colors agree with the original mean color within ± 0.017. The new standard deviation of the colors

tended to increase by 0.079 ± 0.015 compared with the original color standard deviation.

Furthermore, we studied whether the observed decreasing trend of colors with fainter magnitudes is still present with the additional rotation term. We calculated the best-fitted slopes of mean $g - i$ colors versus absolute magnitudes with a bin size of 1 mag. We found that the slopes tend to stay at a mean of -0.02 with a large standard deviation of 0.02. The negative slope is still present, and the additional rotation did not change the results. A larger standard deviation is expected as we added the extra deviations into the colors. From the above tests, we concluded that the average of rotation term $\langle \text{rot} \rangle$ is close to zero, and $\langle C_{\text{obs}} \rangle \sim \bar{C}$, which means the mean observed color is very close to the mean color of the Trojan sample.

The rotational effect also explains the larger color scattering in the DES data. As shown in Figure 4, the DES L5 Trojans have $g - i$ colors have some extremes in both very red ($g - r > 1$) and very blue ($g - r < 0.6$) ends. In contrast, SDSS MOC-4 Trojans all lie in a very narrow range of colors. A simple explanation is that, unlike the DES data, SDSS colors were taken simultaneously, therefore, the scattering of SDSS colors is pure intrinsic color dispersion (σ). On the other hand, the scattering of DES colors is intrinsic color dispersion plus a rotational effect, as we described in Equation (5). To test this explanation, we ran two samples K-S test between the $g - i$ color dispersion distribution of the SDSS and DES samples and obtained a p-value of 0.004, which means the two $g - i$ color dispersion distributions are likely different from each other. This result was expected, because we compared the σ_{sdss} to the $\sigma_{\text{DES}} + \text{rot}_{\text{DES}}$. Then, we added the simulated rotational terms into the SDSS sample. The K-S test returned a p-value of 0.285, which means the color dispersion distributions were now indistinguishable. From the above test, we concluded that the larger color scattering in the DES data was likely induced by the rotational effect. The test also means that any other source of random additional photometric variance with similar uncertainties, e.g., different noise levels on observations of colors, is plausible to account for the difference between SDSS and DES colors.

We note that our function for the amplitudes is not perfect. Some Trojans do have light-curve amplitudes larger than the 0.2 mag mean value that we have assumed above. Nevertheless, these larger light-curve amplitudes are not common, as only ∼5% of identified Trojans have amplitude larger than 0.4 mag (Mottola et al. 2011). We maintain that our approximation is sufficient for the analysis.

4.5. Taxonomic Classification of Jupiter Trojans

Generally, we expect the majority of Trojans to be D-type (red), P-type, or C-type (less-red) asteroids (DeMeo & Carry 2013). However, most of their classifications are based on Trojans in the SDSS and WISE data, which mostly have diameters >20 km. The diameters of most Trojans in the DES data are smaller than that limit. This allows us to probe into the spectral types of a large sample of Trojans with diameters from 5 to 20 km.

In this section, we classify the detected Jupiter Trojans into different classes according to their colors following DeMeo & Carry (2013) classification, which used the spectral slope calculated from g, r, and i reflectance values (gri slope) and $i - z$ colors. The DES photometric magnitudes have been converted to SDSS photometric magnitudes as described in
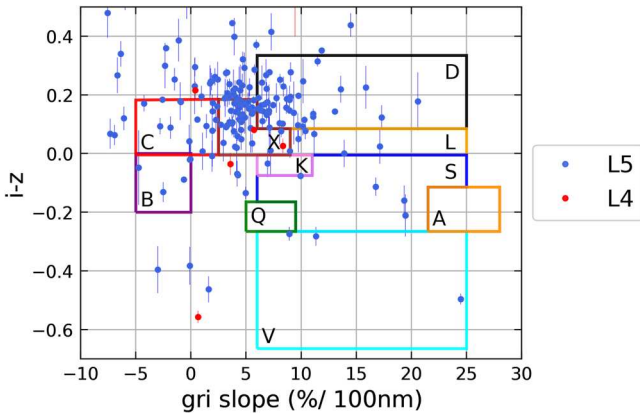
Figure 5. The classification of taxonomy for Jupiter Trojans. Each boundary represents a different class.

Section 4.3. Only Trojans with measurements in all *griz* bands were classified, which include 178 L5 Trojans and 8 L4 Trojans as mentioned in Section 3.4.

Figure 5 shows the distribution of the 186 Trojans on *gri* slope versus $i - z$ diagram. The Trojans are mostly located in X- and D-type regions, and the X-type region contains three degenerate classes E, M, and P. The large scattering is likely to be caused by the rotational effect (see Section 4.4). The center of the distribution is located in the X-type region, which may indicate that in the range of $13 < H < 15$ or in a diameter size range of 5–13 km (assuming albedo = 0.07), there are more P-type Trojans than D-type. Such result is consistent with DeMeo & Carry (2014), which also shows that there are more P- and C-type Trojans than D-type in the smaller size range. As the P- and C-type are less red than the D-type (shallower *gri* slope), this result is consistent with what we found: the mean color is less red for smaller size Trojans.

The amplitudes of asteroid rotations are generally around 0.2 mag (Mottola et al. 2011). Other than the color uncertainties from asteroid rotation, the intrinsic $i - z$ color uncertainties are usually around 0.04 mag. Figure 5 include the intrinsic $i - z$ color uncertainties. Thus, Trojans with exotic taxonomic types, e.g., S- and V-type, should be confirmed with further studies. The difference among C-, X-, and some D-type Trojans is very subtle, primarily dependent on the *gri* slope, as seen in Figure 5. The uncertainties in slopes average on 2%.

5. Discussion

Since the fit of L5 Trojans mean $g - i$ colors in Figure 4 is 0.83 mag at H of 9 mag and 0.75 mag at H of 18 mag and agrees very well with the mean $g - i$ colors of the red (mean = 0.86 mag) and less red (mean = 0.73 mag) populations in SDSS MOC-4 data, which are obtained by fitting a two-peaked Gaussian distribution by Wong & Brown (2015). The increasing fraction of P- and C-type asteroids compared with D-type asteroids is also consistent with the increasing number of less-red objects; as P- and C-type asteroids have smaller *gri* slopes than D-type asteroids. These two pieces of information hint strongly that two distinct populations with different size distributions and surface properties are responsible for the color bimodality of Trojans, with more P- and C-type or less-red asteroids for smaller Trojans.

One hypothesis for the color–size correlation is that red populations were converted to the less-red population as they become fragments (Wong & Brown 2016), exposing fresher

surfaces. They proposed that collisional fragments of both red and less-red groups become less red in colors due to lack of CH_3OH and H_2S. However, further spectroscopic study has not identified any discernible feature in Jupiter Trojans (Wong et al. 2019). It is also possible that the color dichotomy is mainly caused by the difference in surface properties between the two populations. Since the two populations have different size distributions (Wong et al. 2014) and the less red are more populated than the red group in the smaller end, the color–size correlation reported in Wong & Brown (2015) and this work would be an observational consequence of this fact. Nevertheless, whatever mechanisms created the color–size correlation of Jovian Trojans, it must be a general effect between L4 and L5, as both L4 and L5 Trojans share the same color–size trend. Finally, the color–size correlation was not obvious in the colors of $i - z$ and $r - i$ in the DES data compared with $g - i$ and $g - r$ colors. Both $i - z$ and $r - i$ colors were almost constant with magnitudes. This is consistent with the fact that the slope of the reflectance spectrum between the red and less-red groups tends to get closer in longer wavelength (Emery et al. 2011).

6. Summary

We extracted the known Jovian Trojans from the DES data set using their orbital parameters in the MPC database. After excluding stationary objects, constraining uncertainties in the positions and photometry, and removing unstable asteroids, we reach a catalog of 547 unique L5 Trojans and 26 unique L4 Trojans. Using this sample, we study the color distributions of known Trojans in DES data with a focus on L5 Trojans. The color of $g - i$ and $g - r$ decreases with smaller sizes of the L5 Trojans, which is similar to the same color–size trend found in the L4 Trojans (Wong & Brown 2015). We find no obvious correlations between $r - i/i - z$ colors and size of L5 Trojans from the range of $11 < Hr < 15$. Combining the colors derived for DES Trojans with the Trojans from the SDSS MOC-4 data catalog and L4 Trojans from Wong & Brown (2015), we find strong evidence for the color–size correlation of Jovian Trojans, down to absolute magnitudes of $H = 18$. Finally, we classify taxonomic types of L5 Trojans and find more potential C- and P-type (less-red colored) than D-type (red-colored) asteroids at diameters of 5–20 km. The increasing number of C- and P-type Trojans is consistent with their color–size correlations, which show that more less-red colored Trojans are at the small-sized end.

Future surveys are needed to understand the physical properties and mechanics responsible for the correlations in taxonomic classes/colors and sizes of Jupiter Trojans. We expect that the Lucy mission will greatly enhance our knowledge of the composition of Jupiter Trojans.

Facility: DECam.

Software: Spacerock (Napier 2020), Astropy (Robitaille et al. 2013; Astropy Collaboration et al. 2018), SciPy (Virtanen et al. 2020), Numpy (Harris et al. 2020), Matplotlib (Hunter 2007), Pandas (McKinney 2010).

Appendix
Color Conversion between Subaru/Suprime-Cam and SDSS Photometric System

To convert from Subaru/Suprime-Cam g_{sc}, i_{sc} magnitudes to SDSS g_{sdss}, i_{sdss}, we evaluate the linear color conversions between the two systems using in-frame background stars matched in the SDSS DR12 catalogs. We select the SDSS sources with $g_{sdss} < 21$, $i_{sdss} < 21$, and $0 < (g-i)_{sdss} < 2.5$ to this evaluation. Then, we solve the following equation:

$$m_{sc} = m_{sdss} + C\,(g-i)_{sdss}. \tag{A1}$$

Here, m_{sc} and m_{sdss} are the Subaru and SDSS magnitude, respectively, and C is a linear color term. By solving this equation using the in-frame SDSS sources, which consist with $\sim$10,000 of individual g-band measurements and $\sim$35,000 i-band measurements, we find:

$$g_{sc} = g_{sdss} - 0.03(g-i)_{sdss}, \tag{A2}$$

and

$$i_{sc} = i_{sdss} - 0.02(g-i)_{sdss}. \tag{A3}$$

Combining Equation (A2) and Equation (A3), we have

$$(g-i)_{sc} = 0.99(g-i)_{sdss}. \tag{A4}$$

As the $g-i < 1$ for most of Trojans, the errors induced by color conversions between Subaru and SDSS photometry systems are less than 1%. Therefore, we conclude that the effect of color term is negligible.

ORCID iDs

Jiaming Pan (潘嘉明) ● https://orcid.org/0000-0001-9685-5756
Hsing Wen Lin (林省文) ● https://orcid.org/0000-0001-7737-6784
David W. Gerdes ● https://orcid.org/0000-0001-6942-2736
Kevin J. Napier ● https://orcid.org/0000-0003-4827-5049
Jichi Wang (王骥驰) ● https://orcid.org/0000-0002-3102-9442
T. M. C. Abbott ● https://orcid.org/0000-0003-1587-3931
M. Aguena ● https://orcid.org/0000-0001-5679-6747
S. Allam ● https://orcid.org/0000-0002-7069-7857
O. Alves ● https://orcid.org/0000-0002-7394-9466
D. Bacon ● https://orcid.org/0000-0002-2562-8537
P. H. Bernardinelli ● https://orcid.org/0000-0003-0743-9422
G. M. Bernstein ● https://orcid.org/0000-0002-8613-8259
E. Bertin ● https://orcid.org/0000-0002-3602-3664
D. Brooks ● https://orcid.org/0000-0002-8458-5047
D. L. Burke ● https://orcid.org/0000-0003-1866-1950
A. Carnero Rosell ● https://orcid.org/0000-0003-3044-5150
M. Carrasco Kind ● https://orcid.org/0000-0002-4802-3194
J. Carretero ● https://orcid.org/0000-0002-3130-0204
M. Costanzi ● https://orcid.org/0000-0001-8158-1449
J. De Vicente ● https://orcid.org/0000-0001-8318-6813
S. Desai ● https://orcid.org/0000-0002-0466-3288
I. Ferrero ● https://orcid.org/0000-0002-1295-1132
D. Friedel ● https://orcid.org/0000-0002-3632-7668
J. Frieman ● https://orcid.org/0000-0003-4079-3263
J. García-Bellido ● https://orcid.org/0000-0002-9370-8360
R. A. Gruendl ● https://orcid.org/0000-0002-4588-6517
J. Gschwend ● https://orcid.org/0000-0003-3023-8362
K. Herner ● https://orcid.org/0000-0001-6718-2978
S. R. Hinton ● https://orcid.org/0000-0003-2071-9349

D. L. Hollowood ⓘ https://orcid.org/0000-0002-9369-4157
K. Honscheid ⓘ https://orcid.org/0000-0002-6550-2023
D. J. James ⓘ https://orcid.org/0000-0001-5160-4486
K. Kuehn ⓘ https://orcid.org/0000-0003-0120-0808
N. Kuropatkin ⓘ https://orcid.org/0000-0003-2511-0946
F. Menanteau ⓘ https://orcid.org/0000-0002-1372-2534
R. Miquel ⓘ https://orcid.org/0000-0002-6610-4836
F. Paz-Chinchón ⓘ https://orcid.org/0000-0003-1339-2683
A. Pieres ⓘ https://orcid.org/0000-0001-9186-6042
A. A. Plazas Malagón ⓘ https://orcid.org/0000-0002-2598-0514
A. K. Romer ⓘ https://orcid.org/0000-0002-9328-879X
E. Sanchez ⓘ https://orcid.org/0000-0002-9646-8198
M. Schubnell ⓘ https://orcid.org/0000-0001-9504-2059
I. Sevilla-Noarbe ⓘ https://orcid.org/0000-0002-1831-1953
M. Smith ⓘ https://orcid.org/0000-0002-3321-1432
E. Suchyta ⓘ https://orcid.org/0000-0002-7047-9358
G. Tarle ⓘ https://orcid.org/0000-0003-1704-0781
D. Tucker ⓘ https://orcid.org/0000-0001-7211-5729
A. R. Walker ⓘ https://orcid.org/0000-0002-7123-8943
N. Weaverdyck ⓘ https://orcid.org/0000-0001-9382-5199

References

Abbott, T. M. C., Adamów, M., Aguena, M., et al. 2021, ApJS, 255, 20
Astropy Collaboration, Price-Whelan, A. M., Sipőcz, B. M., et al. 2018, AJ, 156, 123
Bernardinelli, P. H., Bernstein, G. M., Montet, B. T., et al. 2021, ApJL, 921, L37
Bernardinelli, P. H., Bernstein, G. M., Sako, M., et al. 2020, ApJS, 247, 32
Bernardinelli, P. H., Bernstein, G. M., Sako, M., et al. 2022, ApJS, 258, 41
Bernstein, J. P., Kessler, R., Kuhlmann, S., et al. 2012, ApJ, 753, 152
Carvano, J. M., Hasselmann, P. H., Lazzaro, D., & Mothé-Diniz, T. 2010, A&A, 510, A43
Chang, C.-K., Chen, Y.-T., Fraser, W. C., et al. 2021, PSJ, 2, 191
DeMeo, F. E., & Carry, B. 2013, Icar, 226, 723
DeMeo, F. E., & Carry, B. 2014, Natur, 505, 629
DES Collaboration 2005, arXiv:astro-ph/0510346
Drlica-Wagner, A., Sevilla-Noarbe, I., Rykoff, E. S., et al. 2018, ApJS, 235, 33
Emery, J. P., Burr, D. M., & Cruikshank, D. P. 2011, AJ, 141, 25
Flaugher, B., Diehl, H. T., Honscheid, K., et al. 2015, AJ, 150, 150
Fleming, H. J., & Hamilton, D. P. 2000, Icar, 148, 479

Fraser, W. C., Brown, M. E., Morbidelli, A., Parker, A., & Batygin, K. 2014, ApJ, 782, 100
Gerdes, D. W., Jennings, R. J., Bernstein, G. M., et al. 2016, AJ, 151, 39
Gerdes, D. W., Sako, M., Hamilton, S., et al. 2017, ApJL, 839, L15
Grav, T., Mainzer, A. K., Bauer, J., et al. 2011, ApJ, 742, 40
Harris, C. R., Millman, K. J., van der Walt, S. J., et al. 2020, Natur, 585, 357
Hendler, N. P., & Malhotra, R. 2020, PSJ, 1, 75
Holmberg, J., Flynn, C., & Portinari, L. 2006, MNRAS, 367, 449
Holt, T. R., Horner, J., Nesvorný, D., et al. 2021, MNRAS, 504, 1571
Hunter, J. D. 2007, CSE, 9, 90
Ivezić, Ž., Lupton, R. H., Jurić, M., et al. 2002, AJ, 124, 2943
Ivezić, Ž., Tabachnik, S., Rafikov, R., et al. 2001, AJ, 122, 2749
Khain, T., Becker, J. C., Lin, H. W., et al. 2020, AJ, 159, 133
Levison, H. F., Olkin, C. B., Noll, K. S., et al. 2021, PSJ, 2, 171
Lin, H. W., Gerdes, D. W., Hamilton, S. J., et al. 2019, Icar, 321, 426
Mainzer, A., Bauer, J., Grav, T., et al. 2011, ApJ, 731, 53
Marzari, F., & Scholl, H. 1998, Icar, 131, 41
McKinney, W. 2010, in Proc. 9th Python in Science Conf. 445, 56, https://conference.scipy.org/proceedings/scipy2010/pdfs/mckinney.pdf
Morbidelli, A., Levison, H. F., Bottke, W. F., Dones, L., & Nesvorný, D. 2009, Icar, 202, 310
Morbidelli, A., Levison, H. F., Tsiganis, K., & Gomes, R. 2005, Natur, 435, 462
Mottola, S., Di Martino, M., Erikson, A., et al. 2011, AJ, 141, 170
Napier, K. 2020, SpaceRocks, https://github.com/kjnapier/spacerocks
Nesvorny, D., Vokrouhlicky, D., & Morbidelli, A. 2013, AAS/DPS Meeting, 45, 508.03
Popescu, M., Licandro, J., Morate, D., et al. 2016, A&A, 591, A115
Robitaille, T. P., Tollerud, E. J., Greenfield, P., et al. 2013, A&A, 558, A33
Roig, F., & Nesvorný, D. 2015, AJ, 150, 186
Roig, F., Ribeiro, A. O., & Gil-Hutton, R. 2008, A&A, 483, 911
Sergeyev, A. V., Carry, B., Onken, C. A., et al. 2022, A&A, 658, A109
Szabó, G. M., Ivezić, Ž., Jurić, M., & Lupton, R. 2007, MNRAS, 377, 1393
Uehata, K., Terai, T., Ohtsuki, K., & Yoshida, F. 2022, AJ, 163, 213
Virtanen, P., Gommers, R., Oliphant, T. E., et al. 2020, NatMe, 17, 261
Walsh, K. J., Morbidelli, A., Raymond, S. N., O'Brien, D. P., & Mandell, A. M. 2011, Natur, 475, 206
Wong, I., & Brown, M. E. 2015, AJ, 150, 174
Wong, I., & Brown, M. E. 2016, AJ, 152, 90
Wong, I., Brown, M. E., Blacksberg, J., Ehlmann, B. L., & Mahjoub, A. 2019, AJ, 157, 161
Wong, I., Brown, M. E., & Emery, J. P. 2014, AJ, 148, 112
Wong, I., Brown, M. E., & Emery, J. P. 2017, AJ, 154, 104
Yoshida, F., & Nakamura, T. 2005, AJ, 130, 2900
Yoshida, F., & Nakamura, T. 2008, PASJ, 60, 297
Yoshida, F., & Terai, T. 2017, AJ, 154, 71
Yoshida, F., Terai, T., Ito, T., et al. 2019, P&SS, 169, 78